

# Toward a Unified Semantic Loss Model for Deep JS-SCC-based Transmission of EO Imagery

Ti Ti Nguyen, Thanh-Dung Le, Vu Nguyen Ha, Duc-Dung Tran, Hung Nguyen-Kha, Dinh-Hieu Tran, Carlos L. Marcos-Rojas, Juan C. Merlano-Duncan, and Symeon Chatzinotas

*Interdisciplinary Centre for Security, Reliability and Trust (SnT), University of Luxembourg, Luxembourg*

**Abstract**—Modern Earth Observation (EO) systems increasingly rely on high-resolution imagery to support critical applications such as environmental monitoring, disaster response, and land-use analysis. Although these applications benefit from detailed visual data, the resulting data volumes impose significant challenges on satellite communication systems constrained by limited bandwidth, power, and dynamic link conditions. To address these limitations, this paper investigates Deep Joint Source–Channel Coding (DJSCC) as an effective SC paradigm for the transmission of EO imagery. We focus on two complementary aspects of semantic loss in DJSCC-based systems. First, a reconstruction-centric framework is evaluated by analyzing the semantic degradation of reconstructed images under varying compression ratios and channel signal-to-noise ratios (SNR). Second, a task-oriented framework is developed by integrating DJSCC with lightweight, application-specific models (e.g., EfficientViT), with performance measured using downstream task accuracy rather than pixel-level fidelity. Based on extensive empirical analysis, we propose a unified semantic loss framework that captures both reconstruction-centric and task-oriented performance within a single model. This framework characterizes the implicit relationship between JS-SCC compression, channel SNR, and semantic quality, offering actionable insights for the design of robust and efficient EO imagery transmission under resource-constrained satellite links.

## I. INTRODUCTION

Modern Earth Observation (EO) systems increasingly rely on high-resolution imagery to support a wide range of applications, including environmental monitoring, disaster response, agriculture, and land-use analysis [1]. Recent advances in machine learning (ML) have enhanced EO by enabling efficient analysis of complex datasets, improving accuracy and predictive insights [2], [3]. However, the growing resolution and acquisition frequency of EO sensors have led to an unprecedented increase in data volume, posing significant challenges for satellite communication systems. In practical EO missions, especially those involving Low Earth Orbit (LEO) satellites, the transmission of high-resolution imagery is constrained by limited bandwidth, strict power budgets, and dynamically varying channel conditions. As a result, raw EO data often cannot be transmitted reliably or in a timely manner to ground stations equipped with high-capacity AI processors, limiting the effectiveness of downstream EO applications [4].

To address these challenges, semantic communication (SC) has emerged as a transformative paradigm, shifting traditional bit-oriented transmission toward conveying data meaning, thereby reducing overhead and latency in bandwidth-

constrained environments [5], [6]. Among SC approaches, deep joint source–channel coding (DJSCC) has shown strong potential by enabling end-to-end learned mappings that jointly optimize compression and transmission robustness over noisy channels [7]. However, deploying DJSCC in EO systems introduces new challenges. Unlike conventional communication systems, whose performance can be optimized using well-defined metrics such as bit error rate or signal-to-noise ratio, SC performance depends on how transmission impairments affect application-level outcomes. Recent works [8]–[10] investigate semantic loss models; however, the implicit and highly coupled relationships among DJSCC compression parameters, channel conditions, and semantic quality remain poorly understood. Specifically, [8] models distortion in SC systems as the sum of two independent components, namely source distortion and channel distortion. The work in [9] adopts a generalized logistic function to approximate semantic similarity; however, this formulation cannot fully capture the two-dimensional characteristics of SC systems. In contrast, [10] adopts a relatively simple sum of exponential term to approximate the average data reconstruction error. Overall, the lack of tractable and expressive models complicates system design, particularly when balancing image reconstruction quality against downstream task performance.

In this work, we investigate two complementary aspects of deploying DJSCC for EO systems. First, a reconstruction-centric DJSCC framework is analyzed, where performance is measured in terms of the visual fidelity of reconstructed images under varying compression ratios and channel signal-to-noise ratios (SNRs). Second, a task-oriented DJSCC framework is developed by integrating DJSCC with lightweight, task-specific machine learning models, such as EfficientViT, deployed at computationally capable ground stations. In this setup, performance is evaluated using application-level metrics that reflect the utility of the received data for EO tasks, rather than pixel-level similarity.

Building on our prior work on SC using the DVB-S2 standard [11], we extend the analysis to systems employing DJSCC. Leveraging extensive empirical evaluations on real-world EO data, we propose a unified data-driven semantic loss model that captures both reconstruction-centric and task-oriented performance within a common framework. Specifically, we utilize the EuroSAT dataset [12] for land use and land cover classification, and evaluate DJSCC performance with

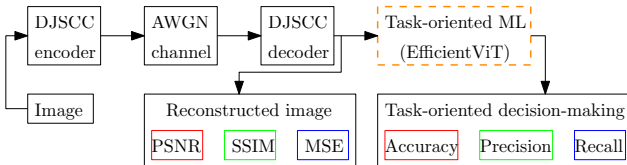


Fig. 1: Block diagram of SC with DJSCC.

and without EfficientViT [13] under varying source compression and channel conditions. The proposed model empirically characterizes the relationship among DJSCC compression settings, channel SNR, and semantic effectiveness. This unified semantic performance framework provides practical guidance for designing robust, bandwidth-efficient, and task-aware EO communication systems.

## II. DATA ACQUISITION FOR SEMANTIC-LOSS MODELING

### A. DJSCC-based Transmission for EO Systems

In this paper, we explore the performance of employing DJSCC in transmitting the EO imagery from satellites to the ground. Specifically, images captured by EO satellites (i.e., the original dataset) are transmitted to ground stations for processing on co-located servers. The images are assumed to be transmitted using the DJSCC technique [7]. The images are then reconstructed at the ground station. Classification is then exploited as a well-known application using these reconstructed images for the performance evaluation.

Unlike traditional communication systems that rely on separate source coding (e.g., JPEG2000) and channel coding (e.g., LDPC or Turbo codes), DJSCC leverages deep neural networks to jointly learn both encoding and decoding functionalities in a single end-to-end model. This enables DJSCC to more effectively preserve semantic information under bandwidth and channel constraints, particularly in non-ideal communication environments where the separation theorem does not hold.

As illustrated in Fig. 1, performance degradation in SC systems using DJSCC stems from two primary sources: (1) source distortion introduced by the encoder-decoder compression process, and (2) channel distortion caused by noisy wireless transmission. To analyze and quantify these effects, we introduce two key parameters: (a) the compression ratio  $\rho$ , defined as the ratio of the size of the original image to the size of the encoded feature vector, and (b) the signal-to-noise ratio (SNR)  $\gamma$ , which characterizes the physical channel quality.

### B. Original Dataset and DJSCC Implementation

The public benchmark for land use and land cover classification dataset, EuroSAT [12], will be used in this study. This is a large-scale benchmark dataset designed explicitly for land use and land cover classification derived from Sentinel-2 satellite imagery. It comprises 27,000 geo-referenced labeled images, each measuring 64x64 pixels and spanning 13 spectral bands. The dataset is categorized into 10 classes. Each class contains 2000–3000 images, including industrial buildings, residential buildings, annual crops, permanent crops, rivers, seas and lakes, Herbaceous vegetation, highways, pastures, and forests across Europe. Due to its compact image size and diverse

TABLE I: EMPIRICAL RESULTS USING DJSCC.

$\gamma \setminus \rho$	2	4	6	8	12
PSNR					
8 dB	35.1659	34.5505	34.0580	33.6110	33.2048
4 dB	34.6355	33.7960	33.1808	32.7066	32.1396
0 dB	33.9541	32.9471	32.2797	31.6707	30.9957
-1 dB	33.6718	32.6668	31.9636	31.4396	30.7259
-2 dB	33.3420	32.4279	31.7131	31.0607	30.3161
-3 dB	33.0512	32.0707	31.3065	30.7091	29.9191
-4 dB	32.7076	31.7420	30.9968	30.3004	29.4664
-5 dB	32.4621	31.3836	30.5894	29.9658	29.0585
-6 dB	32.0890	31.0723	30.2680	29.5925	28.6726
-7 dB	31.8650	30.7567	29.9635	29.2635	28.3096
SSIM					
8 dB	93.9029	93.0065	92.0605	90.8419	89.3904
4 dB	92.8318	91.0260	89.9122	88.5497	86.9133
0 dB	91.4196	88.2488	86.1295	84.2376	81.8966
-1 dB	90.7393	87.6952	85.3222	83.4208	80.6235
-2 dB	90.2920	86.7390	84.0706	81.7849	78.9081
-3 dB	89.2889	85.2669	82.4933	80.2096	76.8448
-4 dB	88.2929	83.8135	80.8698	78.0683	74.5515
-5 dB	86.9725	82.3352	78.8621	76.3074	72.1772
-6 dB	85.5012	80.6746	77.0950	74.1351	69.7947
-7 dB	84.3367	78.9294	75.2783	72.1513	67.5156
MSE					
8 dB	30.1747	35.2691	40.1839	47.5344	58.4974
4 dB	36.4795	48.8558	55.1101	63.4826	76.4652
0 dB	44.4293	64.2171	77.8224	88.3959	106.3604
-1 dB	49.6283	65.6896	78.7179	90.9191	111.2500
-2 dB	50.5202	71.9030	86.6523	102.2033	123.2206
-3 dB	57.5215	80.8606	97.6941	111.2566	134.7072
-4 dB	63.0393	89.4421	106.4504	126.8159	151.5233
-5 dB	70.4309	99.1093	122.2410	136.6730	167.8200
-6 dB	80.5933	110.0527	134.3242	153.9908	185.4238
-7 dB	87.7364	123.5263	147.7795	170.0484	204.4302

class representation, EuroSAT is particularly well-suited for developing and evaluating DL models intended for onboard satellite processing in EO missions. This makes it a valuable resource for applications such as real-time environmental monitoring, disaster response, and precision agriculture.

To evaluate SC performance, we implement the DJSCC framework proposed in [7] under different compression ratios  $\rho$  and SNR  $\gamma$  are considered. Specifically, we consider  $\rho \in \{2, 4, 6, 8, 12\}$  and  $\gamma \in \{-6, -5, -4, -3, -2, -1, 0, 4, 8\}$  (dB). Furthermore, motivated by recent findings in [14], which identify EfficientViT [13] as a highly effective Vision Transformer for EO image classification due to its strong trade-off between performance and computational efficiency, we adopt EfficientViT as the downstream classifier in our evaluation. Accordingly, for each combination of compression ratio  $\rho$  and SNR  $\gamma$ , we apply the DJSCC framework with and without EfficientViT. Our empirical results (shown in Tables I and II) confirm that both  $\rho$  and  $\gamma$  jointly influence semantic performance metrics, including both reconstruction fidelity and task-oriented accuracy. Note that *peak signal-to-noise ratio (PSNR)*, *mean squared error (MSE)*, and *structural similarity index measure (SSIM)* are used to assess image reconstruction quality, whereas *accuracy*, *precision*, and *recall* are considered for evaluating task performance.

$$\xi = \mu_0 + \sum_{i=1}^{N_c} \left( \mu_{1,i} + \frac{\mu_{2,i}}{1 + \exp(-\mu_{3,i}\gamma - \mu_{4,i})} \right) (\exp(\mu_{5,i}\rho) + \mu_{6,i}\rho). \quad (1)$$

TABLE II: EMPIRICAL TASK-LEVEL RESULTS (%) USING EFFICIENTViT-DJSCC.

$\gamma \setminus \rho$	2	4	6	8	12
Accuracy					
8 dB	97.7051	97.2967	96.9067	96.5121	95.8632
4 dB	97.2928	96.5092	96.0357	95.3670	94.3556
0 dB	97.0890	95.6177	94.5010	93.4146	91.3953
-1 dB	96.8802	95.3873	93.9642	92.7888	90.1026
-2 dB	96.6108	94.8307	93.1518	91.5226	88.5643
-3 dB	96.0471	93.7941	92.0042	90.1831	86.5272
-4 dB	95.4615	92.9421	90.5939	88.3597	84.3994
-5 dB	94.7738	91.9048	89.0595	86.6307	81.8966
-6 dB	93.9276	90.6833	87.5220	84.6269	79.1926
Precision					
8 dB	97.6660	97.3024	96.9487	96.5824	95.9765
4 dB	97.2554	96.5211	96.0831	95.4476	94.4837
0 dB	96.8145	95.6488	94.5692	93.5293	91.5745
-1 dB	96.8520	95.3238	94.0368	92.8982	90.2869
-2 dB	96.5923	94.8722	93.2397	91.6484	88.7577
-3 dB	96.0325	93.8358	92.1079	90.3163	86.7739
-4 dB	95.4552	92.9980	90.7076	88.5351	84.6581
-5 dB	94.7731	91.9842	89.1803	86.8053	82.1347
-6 dB	93.9442	90.7627	87.6891	84.8078	79.4080
Recall					
8 dB	97.6127	97.2508	96.8902	96.5088	95.8397
4 dB	97.2018	96.4655	96.0222	95.3674	94.3372
0 dB	96.7542	95.5818	94.4970	93.4260	91.3905
-1 dB	96.7982	95.1904	93.9644	92.8050	90.1037
-2 dB	96.5321	94.8024	93.1568	91.5443	88.5721
-3 dB	95.9718	93.7701	92.0142	90.2106	86.5420
-4 dB	95.3896	92.9224	90.6089	88.3929	84.4213
-5 dB	94.7052	91.8891	89.0794	86.6693	81.9252
-6 dB	93.8619	90.6713	87.5462	84.6706	79.2274

### III. METHODOLOGY - CURVE FITTING-BASED MODELING

To the best of our knowledge, there is no theoretical result in the literature for evaluating the EO application objective, particularly in the context of losses arising from source information reduction and wireless transmission. In the absence of theoretical models, we employ a practical data-fitting approach to represent the EO application objective as a non-linear function of  $\rho$  and  $\gamma$ . Generally, choosing data-fitting models to optimize system parameters can impact system performance [15]. A more accurate fitting model typically leads to a more reliable and effective design.

By applying the same techniques as in [11], we introduce the unified loss model as in (1), where  $N_c$  is the number of terms. However, the MATLAB curve fitting tool does not support the multi-dimensional fitting with the structure given in (1). To find the parameters  $\mu_0, \mu_{i,j}, i = 1 : 6, j = 1 : N_c$ , we employ the gradient descent optimization method. The details of this approach are provided in Algorithm 1, where lines 4-5 to determine the fitting values  $\xi$  and the error between the fitted results  $\xi$  and the measured data in Tables I and

#### Algorithm 1 GRADIENT DESCENT FOR SC MODELING

```

1: Initialize: Set parameters  $\mu_i$  and learning rates  $\alpha_i, i = 0 : 6$ , number of terms  $N_c$ , number of iterations  $N$ , measured data matrix  $\mathbf{Y}$  and set of control parameters  $\rho$  and  $\gamma$ .
2: Initialize gradients:  $\text{Grad}_{\mu_0} \leftarrow \mathbf{0}$ , and  $\text{Grad}_{\mu_i} \leftarrow \mathbf{0}$ , for  $i = 1 : 6$ .
3: for iter = 1 to  $N$  do
4:   Compute  $\xi$  as defined in (1).
5:   Compute error matrix:  $\Psi \leftarrow \mathbf{Y} - \xi$ .
6:   for  $i = 1$  to  $\text{length}(s)$  do
7:     for  $j = 1$  to  $\text{length}(q)$  do
8:       for  $k = 1$  to  $N_c$  do
9:         Compute  $\sigma_k \leftarrow \frac{1}{1 + \exp(-\mu_{3,k}\gamma_i - \mu_{4,k})}$ .
10:        Compute  $\eta_k \leftarrow \exp(\mu_{5,k}\rho_j)$ .
11:        Compute  $\beta_k \leftarrow \eta_k + \mu_{6,k}\rho_j$ .
12:        Update gradients: (where  $\epsilon_{ij} = [\Psi]_{i,j}$ )
13:           $\text{Grad}_{\mu_{1,k}} \leftarrow \text{Grad}_{\mu_{1,k}} - 2\epsilon_{ij}\beta_k$ .
14:           $\text{Grad}_{\mu_{2,k}} \leftarrow \text{Grad}_{\mu_{2,k}} - 2\epsilon_{ij}\beta_k\sigma_k$ .
15:           $\text{Grad}_{\mu_{3,k}} \leftarrow \text{Grad}_{\mu_{3,k}} - 2\epsilon_{ij}\beta_k\mu_{2,k}\sigma_k(1 - \sigma_k)\gamma_i$ .
16:           $\text{Grad}_{\mu_{4,k}} \leftarrow \text{Grad}_{\mu_{4,k}} - 2\epsilon_{ij}\beta_k\mu_{2,k}\sigma_k(1 - \sigma_k)$ .
17:           $\text{Grad}_{\mu_{5,k}} \leftarrow \text{Grad}_{\mu_{5,k}} - 2\epsilon_{ij}\eta_k\rho_j(\mu_{1,k} + \mu_{2,k}\sigma_k)$ .
18:           $\text{Grad}_{\mu_{6,k}} \leftarrow \text{Grad}_{\mu_{6,k}} - 2\epsilon_{ij}\rho_j(\mu_{1,k} + \mu_{2,k}\sigma_k)$ .
22:        end for
23:       $\text{Grad}_{\mu_0} \leftarrow \text{Grad}_{\mu_0} - 2\epsilon_{ij}$ .
24:    end for
25:  end for
26:  end for
27:  Update:  $\mu_0 \leftarrow \mu_0 - \alpha_0 \text{Grad}_{\mu_0}$ 
28:  Update:  $\mu_{i,k} \leftarrow \mu_{i,k} - \alpha_i \text{Grad}_{\mu_{i,k}}$ ,  $i = 1 : 6$ ,  $k = 1 : N_c$ .
29: end for
30: Output: Final parameters  $\mu_i$ ,  $i = 0 : 6$ .

```

II, which is denoted as  $\mathbf{Y}$ . Lines 6 – 26 are to compute the gradients of  $\xi$  with respect to  $\mu_i, i = 0 : 6$ , while lines 27 and 28 are to update  $\mu_i, i = 0 : 6$ . In this paper, we set  $\alpha_0 = \alpha_1 = \alpha_2 = 10^{-4}$ ,  $\alpha_3 = \alpha_4 = 10^{-9}$ , and  $\alpha_5 = 10^{-10}$ . The fitting model parameters corresponding to the results illustrated in Figs. 2 and 3 are given in Tables IV and V IV, respectively.

Figs. 2 and 3 show that the proposed loss model fits well across all considered scenarios, including six different metrics (i.e., PSNR, MSE, SSIM, accuracy, precision, and recall) and two evaluation aspects (i.e., image reconstruction and image classification). Furthermore, we compare our approach with existing loss models to evaluate the fitting capability of the proposed unified loss model. In particular, the ‘G. Sigmoid’ corresponds to the generalized sigmoid model in [9], while the ‘Sum-Exp’ represents the sum-of-exponential model in [10]. These models are defined as

$$\xi_{\text{GSigmoid},\rho} = \kappa_{1,\rho} + \frac{\kappa_{2,\rho}}{1 + \exp(\kappa_{3,\rho}s + \kappa_{4,\rho})}, \quad (2)$$

$$\xi_{\text{SumExp},\rho} = \kappa_{5,\rho} \exp(\kappa_{6,\rho}s) + \kappa_{7,\rho} \exp(\kappa_{8,\rho}s) + \kappa_{9,\rho},$$

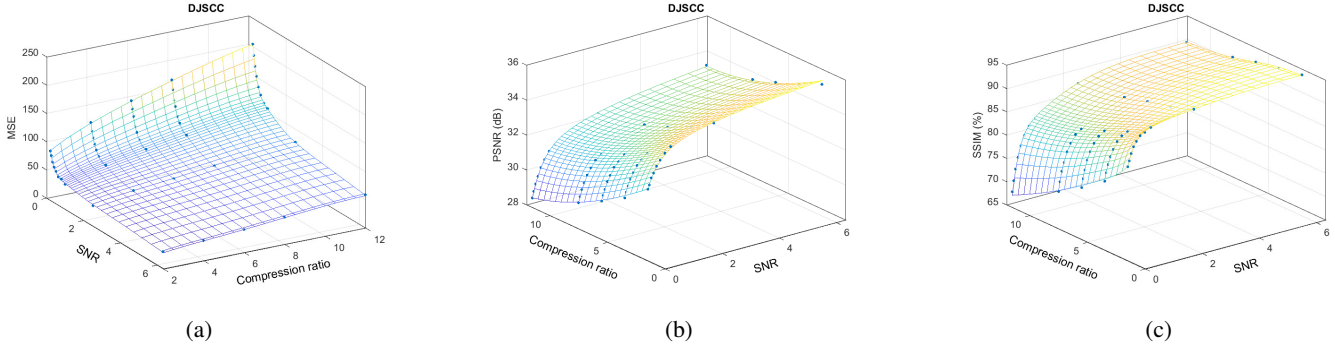


Fig. 2: Curve fitting models for the DJSCC-AWGN case.

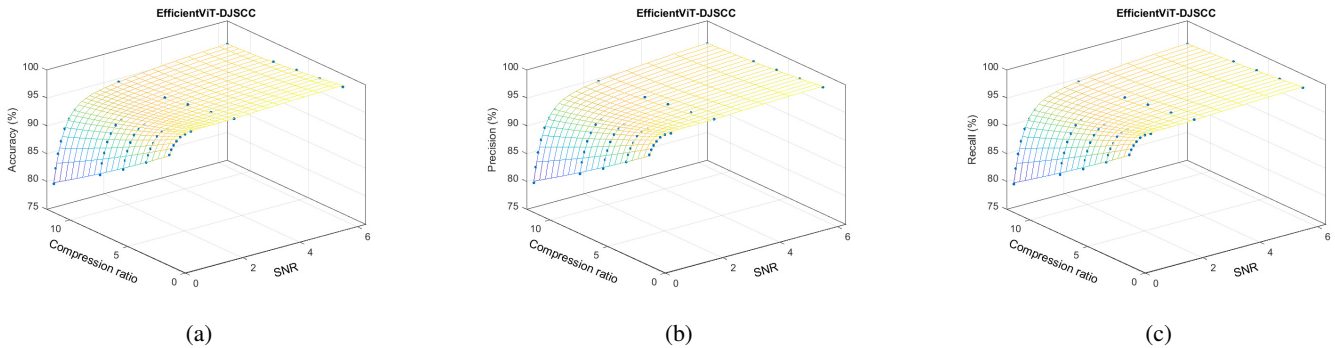


Fig. 3: Curve fitting models for the EfficientViT-DJSCC-AWGN case.

where  $\kappa_{i,\rho}, \forall i$  are determined by fitting to empirical data corresponding to the compression ratio  $\rho$ . It means both  $\xi_{\text{GSigmoid},\rho}$  and  $\xi_{\text{SumExp},\rho}$  are one-dimensional functions of the SNR  $\gamma$ , whereas our proposed model in (1) is a two-dimensional function that jointly depends on  $\rho$  and  $\gamma$ . Since the existing models capture only one-dimensional behavior with respect to SNR  $\gamma$ , we evaluate them by fixing  $\rho = 8$  and  $\rho = 12$ , and then optimally determining the corresponding parameters  $\kappa_{i,\rho}$  for each case. There is no restriction on determining  $\kappa_{i,8}$  and  $\kappa_{i,12}$ . Fig. 4 and Table III illustrate the accuracy results obtained by applying DJSCC with EfficientViT. Our proposed model significantly outperforms both the ‘G. Sigmoid’ and ‘Sum-Exp’ models, even while capturing both dimensions simultaneously.

TABLE III: Average MSE between the measured data and the fitted values.

	Proposed	G. Sigmoid	Sum-Exp.
$\rho = 12$	0.0407	0.2474	0.0521
$\rho = 8$	0.0219	0.1425	0.1133

#### IV. CONCLUSIONS

This work presents a novel data-fitting framework for modeling SC with DJSCC for EO imagery. In particular, it captures the relationship among the EO objective, compression ratio, and channel transmission conditions. By integrating real-world datasets and application-specific insights, the proposed

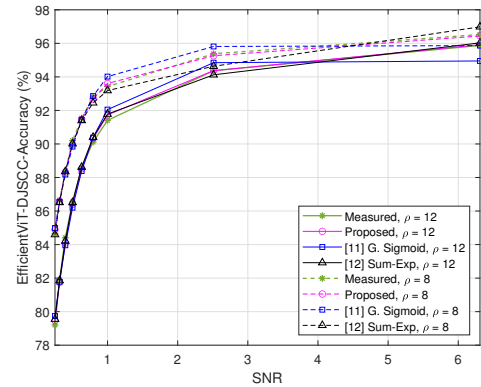


Fig. 4: A comparison of different fitting models.

framework provides a comprehensive approach for modeling SC with DJSCC in EO scenarios. Furthermore, comparisons with existing loss models confirm the strong fitting capability and superior performance of the proposed unified model.

#### REFERENCES

- I. Leyva-Mayorga *et al.*, “Satellite edge computing for real-time and very-high resolution earth observation,” *IEEE Trans. Commun.*, vol. 71, no. 10, pp. 6180–6194, 2023.
- G. Fontanesi *et al.*, “Artificial intelligence for satellite communication and non-terrestrial networks: A survey,” *arXiv preprint arXiv:2304.13008*, 2023.
- M. Affek and J. Szymański, “A survey on the datasets and algorithms for satellite data applications,” *IEEE J. Sel. Topics Applied Earth Observ. Remote Sensing*, 2024.

TABLE IV: PARAMETERS OF THE PROPOSED MODEL IN FIG. 2 UNDER DJSCC-AWGN CONDITIONS.

$i \setminus$ Parameters	$\mu_0$	$\mu_{i,1}$	$\mu_{i,2}$	$\mu_{i,3}$	$\mu_{i,4}$	$\mu_{i,5} \times 10^3$	$\mu_{i,6}$	
<b>Image-MSE</b>								
1	-132.851	325.366	-308.162	-2.900	-2.386	-267.139	0.000	
2		-206.275	549.240	2.640	-0.632	61.433	0.000	
3		-284.726	-194.664	-1.172	-0.607	-328.019	0.000	
4		-161.191	204.884	-0.080	1.757	38.637	0.000	
5		-65.899	61.225	2.840	5.172	222.567	0.000	
6		929.199	-1160.623	2.247	0.330	57.890	0.000	
<b>Image-PSNR</b>								
1	29.574	36.649	-3.168	0.632	-3.436	-39.516	0.000	
2		-104.058	-4.692	0.156	-13.865	-12.833	0.000	
3		-11.463	65.229	2.657	3.110	22.610	0.000	
4		-55.011	-4.879	-0.433	1.825	19.184	0.000	
5		-26.117	28.747	-0.269	20.030	-7.904	0.000	
6		75.898	-14.652	-2.346	-2.705	-7.300	0.000	
<b>Image-SSIM</b>								
1	28.768	126.256	-15.514	-1.740	19.184	-308.684	0.000	
2		55.943	-11.283	-0.996	0.955	19.585	0.000	
3		153.574	4.197	-0.213	-7.228	-701.928	0.000	
4		-206.346	16.021	-1.375	1.974	-548.854	0.000	
5		-37.987	6.056	0.664	5.817	-339.823	0.000	
6		-33.014	28.336	4.731	0.568	78.149	0.000	

TABLE V: PARAMETERS OF THE PROPOSED MODEL IN FIG. 3 UNDER EFFICIENTViT-DJSCC-AWGN CONDITIONS.

$i \setminus$ Parameters	$\mu_0$	$\mu_{i,1}$	$\mu_{i,2}$	$\mu_{i,3}$	$\mu_{i,4}$	$\mu_{i,5} \times 10^3$	$\mu_{i,6}$	
<b>EfficientViT-Accuracy</b>								
1	62.683	-128.798	-7.955	0.859	2.765	-1.475	0.008	
2		-16.487	63.019	0.253	3.622	-11.792	0.166	
3		-124.914	4.798	4.230	1.162	-7.734	-0.069	
4		146.847	20.979	-1.989	-0.866	-14.133	-0.112	
5		20.938	-106.143	-3.172	-2.294	5.252	0.113	
6		63.187	15.759	0.622	4.974	2.075	-0.000	
<b>EfficientViT-Precision</b>								
1	62.695	-128.788	-8.028	0.859	2.765	-1.316	0.008	
2		-16.544	62.923	0.253	3.621	-12.244	0.166	
3		-124.869	4.712	4.230	1.162	-8.155	-0.069	
4		146.910	21.145	-1.989	-0.866	-13.233	-0.112	
5		20.899	-106.007	-3.172	-2.294	4.992	0.112	
6		63.198	15.761	0.622	4.974	2.005	-0.000	
<b>EfficientViT-Recall</b>								
1	62.667	-128.816	-7.989	0.859	2.765	-0.928	0.008	
2		-16.551	62.961	0.253	3.622	-12.896	0.166	
3		-124.907	4.735	4.230	1.162	-8.707	-0.069	
4		146.867	21.114	-1.989	-0.866	-11.932	-0.113	
5		20.886	-106.115	-3.172	-2.294	4.889	0.112	
6		63.170	15.741	0.622	4.974	1.814	-0.000	

[4] H.-f. Chou *et al.*, “Edge ai empowered physical layer security for 6g ntn: Potential threats and future opportunities,” *arXiv preprint arXiv:2401.01005*, 2023.

[5] W. Yang *et al.*, “Semantic communications for future internet: Fundamentals, applications, and challenges,” *IEEE Commun. Surveys & Tuts.*, vol. 25, no. 1, pp. 213–250, 2022.

[6] H.-f. Chou *et al.*, “On-air deep learning integrated semantic inference models for enhanced earth observation satellite networks,” *arXiv preprint arXiv:2409.15246*, 2024.

[7] E. Bourtsoulatze, D. B. Kurka, and D. Gündüz, “Deep joint source-channel coding for wireless image transmission,” *IEEE Trans. Cog. Commun. Netw.*, vol. 5, no. 3, pp. 567–579, 2019.

[8] J. Huang, K. Yuan, C. Huang, and K. Huang, “D<sup>2</sup>-JSCC: Digital deep joint source-channel coding for semantic communications,” *IEEE Journal on Selected Areas in Communications*, 2025.

[9] W.-F. Wang, J.-P. Sheu, and N. Van Cuong, “Joint scheduling and relay allocation for semantic and delay-sensitive wireless communications,” *IEEE Trans. Green Commun. Netw.*, vol. 10, pp. 1666–1678, 2025.

[10] G. Ding, S. Liu, J. Yuan, and G. Yu, “Joint URLLC traffic scheduling and resource allocation for semantic communication systems,” *IEEE Trans. Wireless Commun.*, vol. 23, no. 7, pp. 7278–7290, 2023.

[11] T. T. Nguyen *et al.*, “A semantic-loss function modeling framework with task-oriented machine learning perspectives,” *Proc. IEEE Int. Conf. Machine Learn. Commun. Netw. (ICMLCN)*, 2025.

[12] P. Helber, B. Bischke, A. Dengel, and D. Borth, “Eurosat: A novel dataset and deep learning benchmark for land use and land cover classification,” *IEEE J. Sel. Top. Appl. Earth. Obs. Remote Sens.*, vol. 12, no. 7, pp. 2217–2226, 2019.

[13] X. Liu *et al.*, “Efficientvit: Memory efficient vision transformer with cascaded group attention,” *Proc. IEEE Comput. Soc. Conf. Comput. Vis. Pattern Recognit.*, pp. 14420–14430, 2023.

[14] T. D. Le *et al.*, “On-board satellite image classification for earth observation: A comparative study of vit models,” *arXiv preprint arXiv:2409.03901*, 2024.

[15] T. T. Nguyen, V. N. Ha, L. B. Le, and R. Schober, “Joint data compression and computation offloading in hierarchical fog-cloud systems,” *IEEE Trans. Wireless Commun.*, vol. 19, no. 1, pp. 293–309, 2019.